A Self-Sufficient Lipid Transport Protein in *Mycoplasma pneumoniae*

Sina Manger[1,6], Serena M. Arghittu[2,6], Lasse Sprankel[1], Jakob Meier-Credo[3], Konstantin Wieland[1], Daniela Bublak[1], Julian Langer[3], Roberto Covino[2,5*], Achilleas S. Frangakis[1*]

[1]Buchmann Institute for Molecular Life Sciences and Institute for Biophysics, Goethe University, Frankfurt am Main, Germany

[2]Frankfurt Institute for Advanced Studies, IMPRS on Cellular Biophysics, Frankfurt am Main, Germany

[3]Max Planck Institute for Biophysics, Frankfurt, Germany

[5]Institute of Computer Science, Goethe University, Frankfurt am Main, Germany

[6]These authors contributed equally: Sina Manger, Serena M. Arghittu

*Correspondence: A.S.F. (achilleas.frangakis@biophysik.org) and R.C. (covino@fias.uni-frankfurt.de).

Classification

PHYSICAL SCIENCES/Biophysics and Computational Biology

Keywords

Lipid transport protein, lipids, Mycoplasma, molecular dynamics simulations, cryo-electron microscopy

Abstract

Lipid acquisition and transport are fundamental processes in all organisms, but many of the key players remain unidentified. In this study, we investigate the lipid-cycling mechanism of the minimal model organism *Mycoplasma pneumoniae*. We show that the essential protein P116 can extract lipids from the environment but also self-sufficiently deposit them into both eukaryotic cell membranes and liposomes. Our structures and molecular dynamics simulation reveal the mechanism by which the N-terminal region of P116, which resembles an SMP domain, perturbs the membrane, while a hydrophobic pocket exploits the chemical gradient to collect the lipids. Filling of P116 with cargo leads to a conformational change that modulates membrane affinity without consumption of ATP. We show that the Mycoplasmas have one integrated lipid acquisition and delivery machinery that shortcuts the complex multi-protein pathways used by higher developed organisms.

Introduction

All organisms use membranes to enclose their cells and to organize subcellular compartmentalization. Specialized protein-based machineries transport lipids into and between membranes. Several such machineries have been characterized in recent years, such as the synaptotagmin-like mitochondrial-lipid-binding protein (SMP) domains of the ERMES complex, which tethers the endoplasmic reticulum to the mitochondrium[1], and the extended synaptotagmins (E-Syt), which tether the endoplasmic reticulum to the plasma membrane[2,3]. Another example is the maintenance of lipid asymmetry (Mla) pathway, in which the soluble periplasmic protein MlaC acts as a lipid shuttle to maintain the asymmetrical Gram-negative outer membrane via retrograde phospholipid transport[4,5]. These machineries share some similarities between the domains responsible for lipid uptake, binding, and deposition. Typically, membrane perturbation and binding of one or two lipid molecules happens within the same domain. However, whereas MlaC receives lipids from another protein complex, SMP domains are capable of self-sufficient lipid extraction from membranes[2].

The immunogenic and essential protein P116 from *Mycoplasma* was recently found to bind lipids within a large hydrophobic cavity[6]. *Mycoplasma* species belong to the class of Mollicutes and are characterized by the lack of a cell wall, a small genome, and a reduced metabolism, making them a model organism for a minimal cell. *M. pneumoniae* adapts its membrane composition to the lipid composition of the culture medium[7,8], but the underlying mechanisms and proteins involved were unknown. Although a structure has been reported for the Mce1 lipid-import machine of a *Mycobacterium tuberculosis* relative[9], studies on cholesterol uptake by other clinically relevant bacteria, such as *Borrelia burgdorferi* and *Helicobacter pylori*, are largely lacking.

P116 is a homodimer of two 116 kDa monomers, comprising each one core domain, one dimerization domain and one N-terminal domain connected to a transmembrane helix via an unstructured linker. The core domain has a unique fold that resembles a half-open left hand, with four pairs of amphipathic α-helices (the 'finger helices'), a long α-helix and a five-strand β-sheet (the 'palm') forming a huge hydrophobic cavity[6]. The cavity is accessible via the distal core access (DCA), a channel formed between two amphipathic helices, just beneath the N-terminal domain (Supplemental Figure 1a). P116 binds a large variety of lipids, including phosphatidylcholine (PC), sphingomyelin (SM) and sterols, which are growth-limiting for *Mycoplasma pneumoniae*[6]*.* The lipid cargo inside the hydrophobic cavity can be reduced by detergent treatment, yielding a protein in which the volume of the hydrophobic cavity is reduced by 60 percent (Supplemental Figure 1b). However, even in this *empty* state the cavity still contains a small number of lipid molecules. The cavity of the *empty* protein can be refilled with lipids by incubation with serum or HDL[6].

Here, we show that P116 is an integrated machinery that can both acquire and deliver lipids. It used its N-terminal domain, that resembles the fold of the SMP domains, to bind to and perturb membranes. We show that P116 can deliver lipids into phospholipid vesicles and eukaryotic cell membranes independently of other proteins. Molecular dynamics (MD) simulations of P116 details the route of lipid uptake and delivery. Integration of these different approaches reveals that P116 is a compact versatile machinery for lipid extraction and delivery into membranes. Unlike the multi-protein pathways required in more complex organisms, P116 can accomplish these tasks single-handedly.

Results

I. The N-terminal domain folds like an SMP domain and is required to extract lipids from membranes.

Cryo-electron tomograms *of M. pneumoniae* cells display P116

Native P116 is tethered to the mycoplasma membrane. Tomography of wildtype mycoplasma cells display densities at the plasma membrane that resemble P116 (Figure 1a). Proteomics analysis show only ~34 copies of P116[10] on wildtype cells, which, in addition to its low molecular weight of 232 kDa, complicates a structural characterization. To overcome this problem, we generated an *M. pneumoniae* strain that overexpresses *p116* from its native promoter. The tomograms display cells decorated with densities creating a crown-like arrangement on the mycoplasma membrane and resembling P116 (Figure 1*b*). We analyzed the conformation of P116 using sub-tomogram averaging. The resulting average was severely affected by the missing wedge owed to the minute size of particle and the visually discernable flexibility of the individual particles. In the density map only the core and the N-terminal domain could be discerned (Figure 1c).

For further analysis of the properties of P116, we used three different soluble fragments of P116 (Figure 1c & d): (i) The ectodomain missing the transmembrane helix and part of the C-terminus (referred to as P116 30–975), (ii) a fragment of the ectodomain missing its N-terminal domains (referred to as P116 246-818) that was used for lipid binding and delivery assays as well as single particle cryo-electron microscopy (cryo-EM) and (iii) the ectodomain missing the linker region at the N-terminus and another part of the C-terminus, which were segments that could not be

resolved by cryo-EM and are thus absent in the protein PDBs (referred to as P116 60–868, PDBs: 8a9a and 8a9b).

Tomograms of M. *pneumoniae* cells

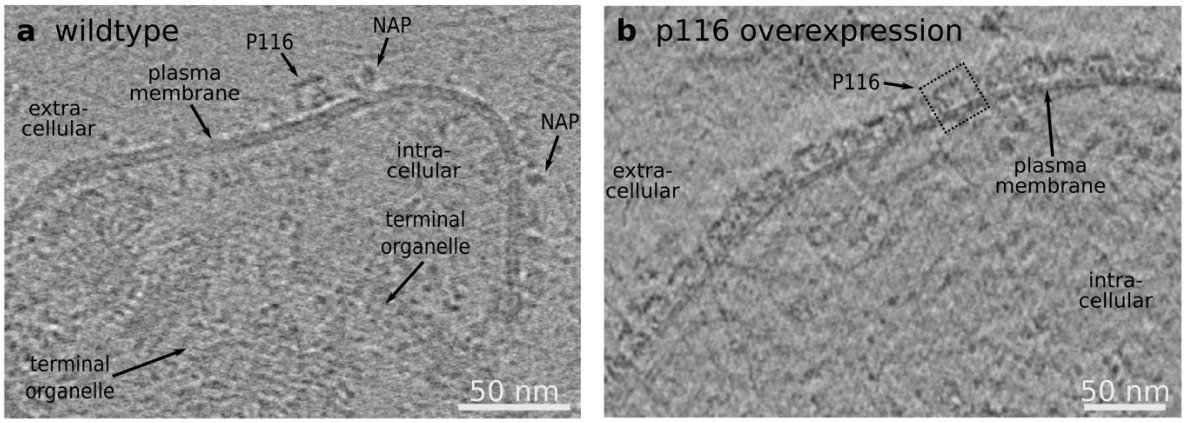

Model of dominant membrane conformation of P116

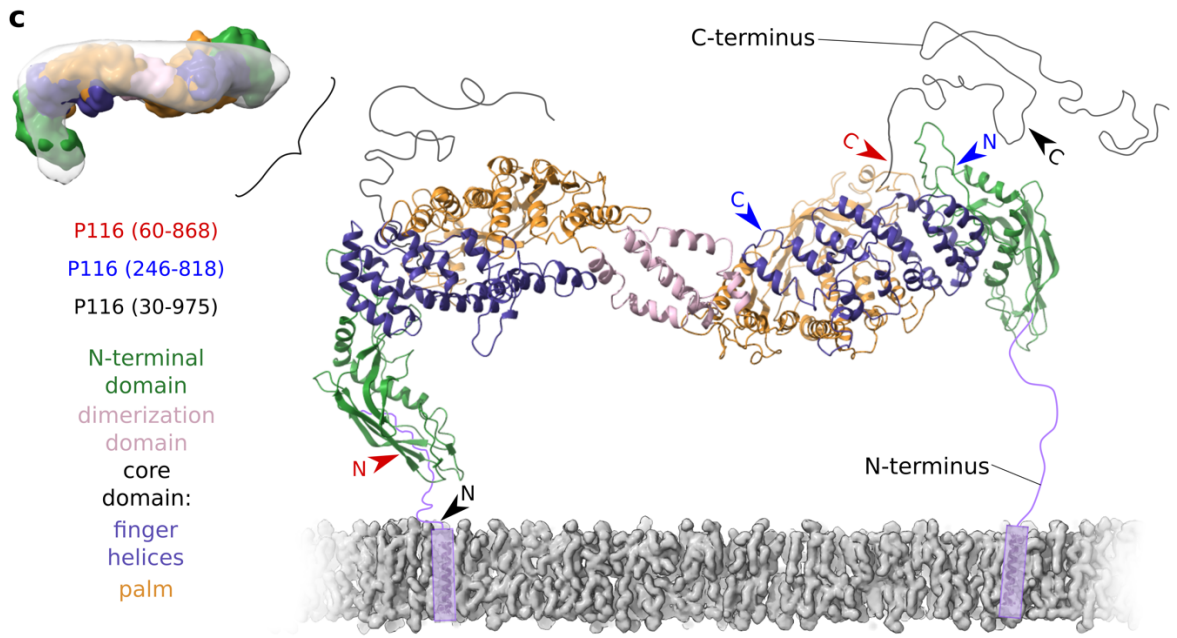

Amino acid sequence of P116

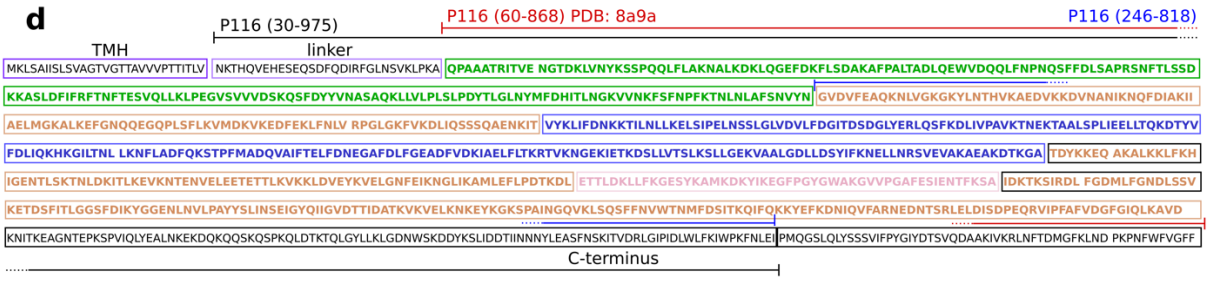

Figure 1: Cryo-electron tomography of *M. pneumoniae* cells display the position of P116.

a, b Computational slices through tomographic reconstructions (0.837 Å/pix) of (a) a wildtype *M. pneumoniae* cell and (b) a cell overexpressing *p116* from its native promoter. In the computational slices the characteristic features of *M. pneumoniae* cells can be seen, such as the terminal organelle in the cytoplasm and several adhesion complexes (NAP) at the plasma membrane. In the wildtype cell just one individual P116 particle can be discerned. In comparison, the cell overexpressing *p116* is decorated with P116 particles that, constrained by their membrane tether, only reach a certain distance to the membrane producing a "crown" around the cell membrane.

c Model of the membrane-tethered conformation of P116 as seen in many P116 particles on the mycoplasma membrane. The sub-tomogram average of 700 particle (primarily side views) (*top left*, Supplemental Figure 7) was fitted using a conformation P116 (P116 60-868, PDB: 8A9A) assumed during MD simulations in the vicinity of a membrane (details on the MD simulation can be found in section III.). The domains are color-coded (N-terminal domain in green, core domain in blue (for the four amphipathic helices) and orange (for the palm), dimerization domain in pink, transmembrane helix in purple, linker in light purple and C-terminus in black) and the ectodomain fragments used in this study are indicated with black (P116 30-975), red (P116 60-868) and blue (P116 246-818) arrows. The transmembrane helix, linker and C-terminus are not structurally resolved and therefor only sketched into the model.

d Amino acid sequence of P116 with the same color scheme that was used for the ribbon model. The ectodomain fragments used in this study are indicated with black (P116 30-975), red (P116 60-868) and blue (P116 246-818) bars.

Purified P116 can self-sufficiently extract lipids from intact membranes

P116 can extract lipids from high-density lipoprotein particles and serum in the presence of other lipid-binding proteins and lipoproteins[6]. Here, we first set out to demonstrate that the ectodomain of P116 (30–975; missing the transmembrane helix and part of the C-terminus) is capable of extracting lipids from intact membranes in the absence of other proteins. We reduced the cargo of P116 by detergent treatment and verified the absence of DPPC in this *empty* state via mass spectrometry (Figure 2a, blue spectrum). Subsequently we incubated the *empty* P116 with dipalmitoylphosphatidylcholine (DPPC) liposomes, which were then removed by two rounds of ultracentrifugation. Analysis of the cargo of P116 by mass spectrometry revealed DPPC bound to P116, which was previously absent in the *empty* P116 (Figure

2a, black spectrum). When we repeated the procedure on a similar mixture of DPPC liposomes with the non-lipid binding mycoplasma proteins P110/P140, no lipids could be detected in the sample by mass spectrometry, showing the absence of liposome carryover after ultracentrifugation (liposome contamination control, Figure 2a, red spectrum). Thus, the soluble ectodomain of P116 can perturb the membrane and extract lipids single-handedly, i.e. without the involvement of any other proteins.

The N-terminal domain resembles conserved lipid shuttle proteins

Next, we investigated the mechanism by which P116 extracts lipids from membranes. Structural comparison shows that the N-terminal domain has a similar fold to other small lipid shuttles such as the sterol carrier protein 2 (SCP2), which appears either isolated or as a part of multidomain proteins in all forms of life[11,12], and the SMP domains, which are part of tether complexes at membrane contact sites in eukaryotes[1,3] (Supplemental Figure 2). Although the comparison of the amino acid sequences of the P116 N-terminal domain and the E-Syt SMP domain shows poor conservation, with only 14% sequence identity and 25% similarity with 55% gaps (Supplemental Figure 2), they share a large antiparallel β-sheet that covers three sides of a hydrophobic channel, while the remaining side is closed by an α-helix (Supplemental Figure 2). Both SCP2 and SMP domains perturb membranes, damaging their integrity and exposing individual lipids to the aqueous environment, and transfer lipids between membranes in a self-sufficient way[2,12]. Thus, we hypothesized that the P116 N-terminal domain is involved in perturbing the membrane.

The N-terminal domain is responsible for perturbing membranes

We severed the P116 N-terminal domain from the rest of the ectodomain to further explore its role in membrane perturbation. We solved the structure of this

truncated P116 construct (246–818) by single-particle cryo-electron microscopy (cryo-EM) at 4.3 Å (according to the gold-standard criterion of Fourier shell correlation (FSC) = 0.143; EMD-50314, PDB: 9FCH; Supplemental Figure 3). The structure resembled the core and dimerization domains of the full-length ectodomain of P116 (30–957; EMD-15274, PDB: 8A9A) (Figure 2b). This shows that the overall structure and domain organization of P116 was not changed by the truncation and that the truncated construct was lipid-filled and thus generally able to bind lipids.

Next, we emptied the truncated P116 construct (246–818) and incubated it with DPPC liposomes, following the identical procedure as above (lipid extraction experiment carried out on the whole ectodomain (P116 30-975). After removing the liposomes by ultracentrifugation, we solved the cryo-EM structure of the truncated P116 construct (246-818) to verify its structural integrity after the experiment and simultaneously determine whether it was filled with lipids. We obtained the structure of the monomer at 5.43 Å (according to the gold-standard criterion of FSC = 0.143; EMD-18478; Supplemental Figure 3) and determined that the monomer was *empty* (Figure 2c, Supplemental Figure 1b). In the empty state, the volume of the hydrophobic cavity is reduced [6]. This happens because helix pair 2 moves towards the inside of the cavity. Thus, the position of helix pair 2 can be used to assess whether the cavity is *full* or *empty* (Supplemental Figure 1b).

Most of the particles in the cryo-EM dataset were monomers, showing that the *empty* truncated construct was prone to break up into monomers. We observed this behavior also in the *empty* full-length ectodomain of P116 (30–975), albeit to a lesser extent. However, the density map we obtained from the less abundant dimers in the dataset matched the conformation of the monomer (EMD-50307, Supplemental Figure 4). This confirms that the observed inability to refill from liposomes was not related to the decay of the dimer. In summary, the experiment showed that in the absence of the

N-terminal domain, extraction of lipids from intact membranes is no longer possible or much less efficient.

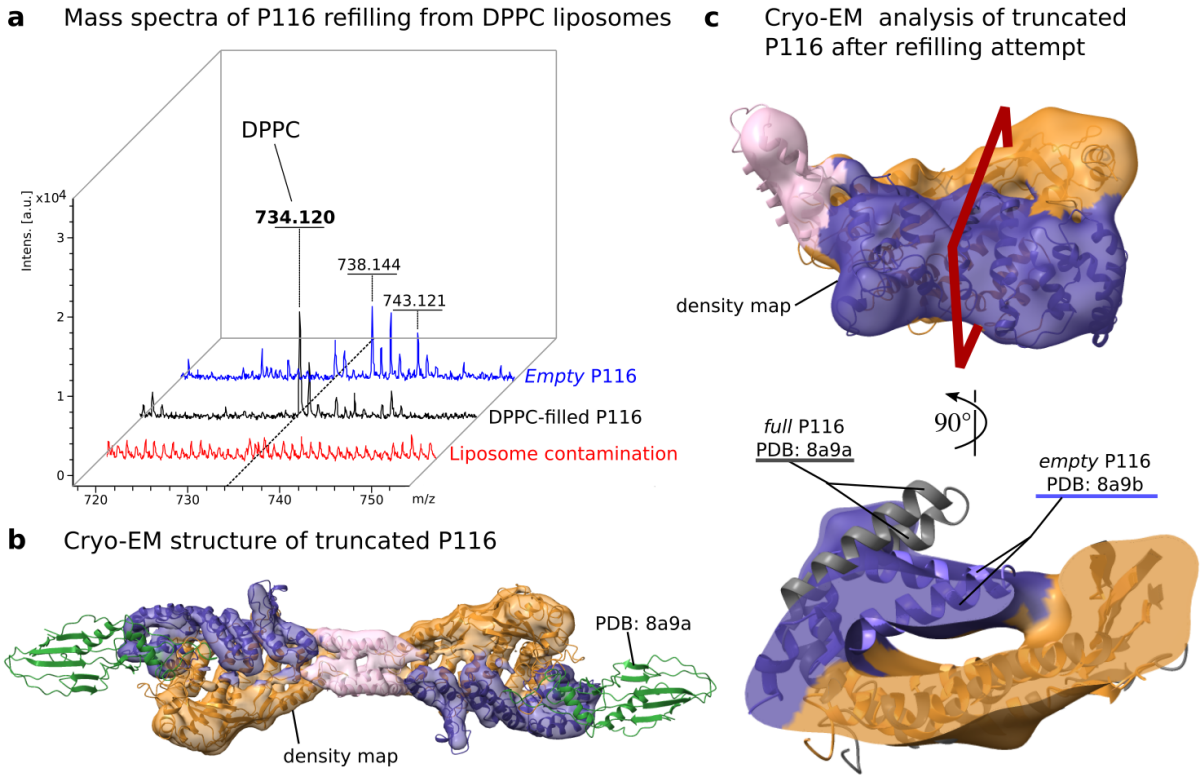

Figure 2: The N-terminal domain of P116 is required to extract lipids from membranes.

a Mass spectrometry analysis of DPPC extraction from liposomes by P116.
In blue: Lipid-depleted (*empty*) P116 (traces of lipids at the masses 738 and 743 Da are visible).
In black: P116 after incubation with and pelleting of DPPC liposomes (a clear peak at 734 Da, the mass of DPPC, is visible).
In red: DPPC carryover after liposome pelleting in control sample with the non-lipid binding mycoplasma proteins P110/P140 (no DPPC liposome contamination is visible).
b Cryo-EM structure of the N-terminal domain truncated P116 has a similar fold to the full-length protein. The isosurface presentation of the cryo-EM density of P116 without the N-terminal domain (246–818) at 4.3 Å resolution (EMD-50314, PDB: 9FCH) superimposed on the ribbon representation of the original structure of the filled full-length ectodomain of P116 (60–868) (PDB: 8A9A).
c Isosurface representation of the cryo-EM density map of the N-terminal domain truncated P116 (246–818) monomer (light purple, light orange) after emptying and attempted refilling superimposed with the ribbon model of the *empty* ectodomain of P116 (PDB: 8A9B) (top). Computational slice of the density map (the position is indicated by the red box) superimposed with the ribbon model of the *full* ectodomain of P116 (grey, PDB: 8A9A) and the *empty* ectodomain of P116 (purple and orange, PDB:

8A9B) (bottom). Helix pair 2 of the filled conformation stands out from the density of the truncated P116 monomer, illustrating that the monomers were not refilled but remained *empty* (compare Supplemental Figure 1b).

II. P116 self-sufficiently delivers lipids

The P116 ectodomain delivers fluorescent lipids into liposomes *in vitro*

Next, we probed whether P116 can deposit lipids into membranes. We established a fluorescence-based assay using liposomes (Figure 3a), whereby *empty* P116 was incubated with small (200 nm) fluorescent donor liposomes. The liposomes comprised 30% DOPE labelled with a Dansyl-fluorophore at the head group, 30% DOPC labelled with an NBD fluorophore in one acyl chain, and 40% DOPG (Figure 3a & c). The donor liposomes were then removed by ultracentrifugation. The suitability of this removal method was confirmed by mass spectrometry of a separate control, in which a non-lipid binding mycoplasma protein (P110/P140) was used instead of P116 (Supplemental Figure 5b), yielding no detectable DPPC in the final sample. The P116 loaded with fluorescent lipids was subsequently incubated with large DPPC acceptor liposomes (> 1 µm) for 2 hours at ambient conditions. In the final step, P116 was removed by ultrafiltration, and its absence was confirmed with a dot blot (Supplemental Figure 5c). The remaining DPPC liposomes were imaged by fluorescence microscopy. The auto-fluorescence of the acceptor liposome was measured along with the fluorescence signal of a control to account for spontaneous transfer of lipids or fusion of liposomes as a result of potential carryover of fluorescent donor liposomes (Figure 3b-d, Supplemental Figure 6).

The DPPC acceptor liposomes displayed an intense fluorescence signal (Figure 3b 1). The signal in both controls was statistically significantly smaller (Supplemental Table 1): in the NBD channel, no signal was detected in either control; while in the

Dansyl channel, both controls displayed some (auto) fluorescence signal. Thus, NBD-DOPC and Dansyl-DOPE were both delivered into the DPPC acceptor liposomes, independently of whether the fluorophore was placed in the head or the tail group. Liposome carryover below the sensitivity range of the mass spectrometry control may be present, and spontaneous transfer was not detected for NBD-DOPC but was found to some extent for Dansyl-DOPE. The absence of an NBD-DOPC signal in the control confirms that fusion of carryover fluorescent donor liposomes and DPPC acceptor liposomes did not occur. Potentially present carryover fluorescent donor liposomes could not have been mistaken for acceptor liposomes, because they are at least five-fold smaller, which is below the resolution limit of the light microscope. The experiment was successfully replicated 3 times. Analysis of the DPPC liposomes with mass spectrometry instead of fluorescence microscopy yielded the same result (Supplemental Figure 5a). Hence, the ectodomain of P116 can deposit its cargo into a phospholipid membrane without being tethered to the mycoplasma membrane and without requiring other proteins.

To explore whether P116 can also deliver its cargo in living cells, we incubated P116 filled with fluorescent lipids together with adherent HaCaT cells in serum-free DMEM medium for 30 minutes at 37°C, before removing the P116 by thorough washing. Subsequent analysis of the cells by fluorescence microscopy revealed intense fluorescence (Figure 3b 2).

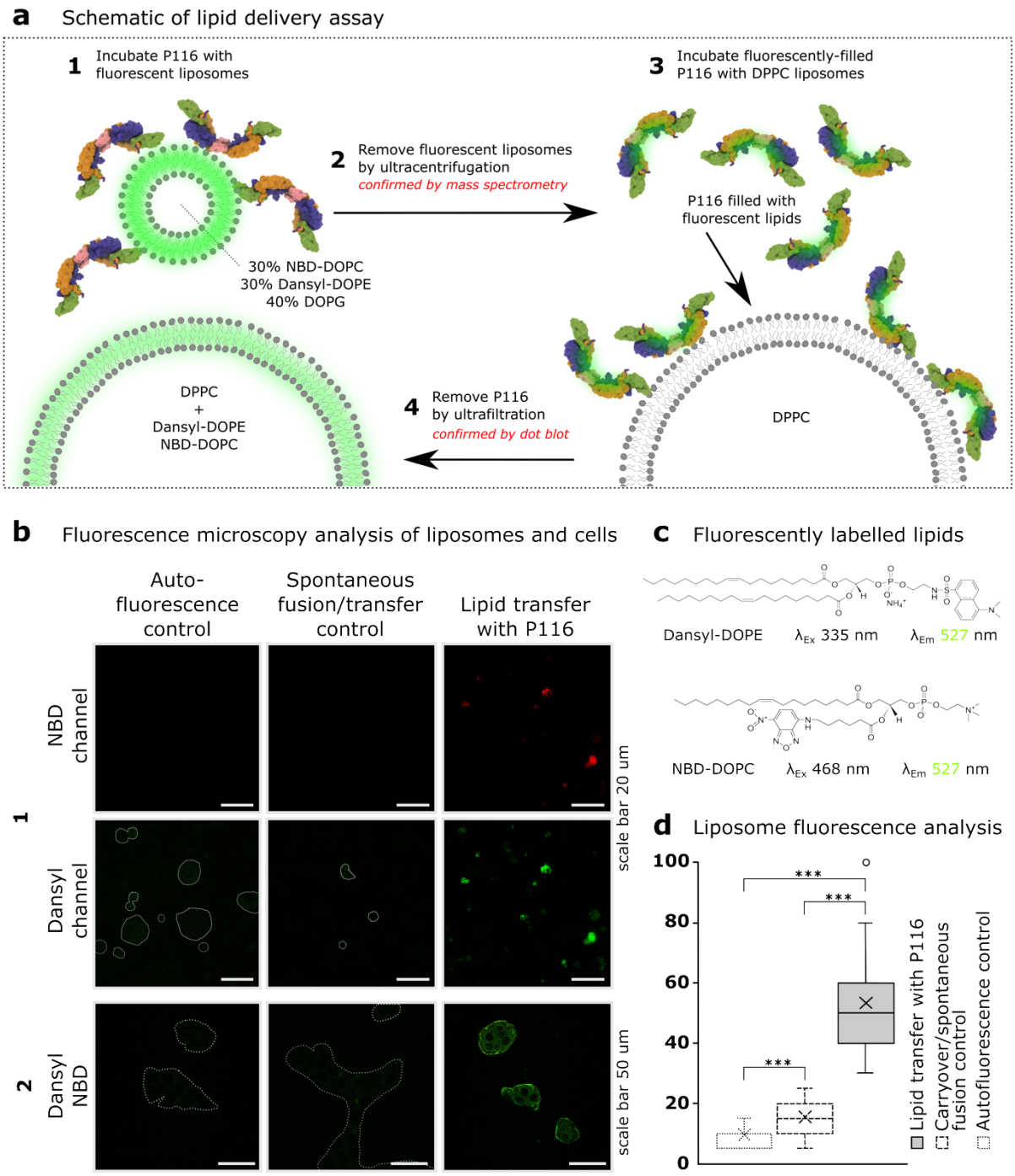

Figure 3: P116 self-sufficiently and single-handedly delivers lipids.
a Schematic of lipid delivery assay. 1) Incubation of *empty* P116 with fluorescent donor liposomes. 2) Removal of donor liposomes by ultracentrifugation and verification of removal by mass spectrometry. 3) Incubation of now fluorescently filled P116 with non-fluorescent DPPC acceptor liposomes. 4) Removal of P116 by ultrafiltration and verification of removal by dot blot, followed by analysis of fluorescent traits of acceptor liposomes by laser-scanning microscopy.
b Representative confocal light microscopy images. 1) Delivery into DPPC liposomes. 2) Delivery into HaCaT cells. (Left) Liposomes/cells (auto-fluorescence control), (middle) sample from the same workflow without P116 (spontaneous fusion/transfer

control), and (right) sample with P116, according to the workflow detailed in **a** (lipid transfer with P116). The Dansyl and NBD channels are shown separately because of the large difference in excitation maxima and resulting use of separate laser lines. Both fluorophores emit in the green spectrum (at 527 nm). The NBD fluorescence signal is shown in red to facilitate interpretation of the merged image.
c Fluorescent lipids used in donor liposomes with their excitation and emission maxima.
d Statistical analysis of fluorescence differences between the sample in the presence of P116 and the controls. All differences are statistically significant. The experiment was carried out in triplicate, and all results could be replicated. The 25–75% data range is contained in the box, the horizontal line represents the median, the vertical line represents range within 1.5 interquartile range, the X represents the mean, and the O represents outlier. Data can be found in Supplemental Table 1.

III. Interaction of P116 with membranes facilitates increased range of motion

The conformational dynamics of P116 depend on its cargo and membrane proximity.

The function of P116 is determined by its interactions with both host and mycoplasma membrane. Thus, we set out to better understand how P116 interacts with membranes and how these interactions modulate its conformational dynamics. As the task requires efficient sampling beyond the microsecond timescale, we performed long equilibrium quasi-atomistic MD simulations of the P116 ectodomain (60–868; PDB: 8A9B; this fragment of P116 was used for all MD simulations) using the MARTINI forcefield. Comprehensive studies showed that MARTINI 3.0 can accurately reproduce protein lipid interactions[13].

Our simulations included *empty* P116 on membrane and in solution. To compare the membrane association at different filling states, we also simulated the model of *full* P116 on a membrane. We chose a membrane composition consistent with the liposomes used in the lipid transfer experiment (30% DOPC/30% DOPE/40%

DOPG). Our MD simulations showed a broad range of motion, involving changes to the arc diameter (distance between the monomers), the wringing angle (rotation of the monomers with respect to each other), and the interdomain angle between the N-terminal domain and the core domain (Supplemental Figure 1c).

(i) Wringing angle (Figure 4a): Simulated *empty* P116 in solution displayed an average wringing angle of 40° ± 20°, allowing the monomers to face in the same directions (down-down). This range qualitatively resembled the wringing observed in the cryo-EM structures[9], which ranged from -20° to 30°. In contrast, simulated *empty* P116 on a membrane displayed a far increased wringing angle of 80° ± 20°, which enables the monomers to face opposite directions (up-down) (Figure 4a, *left*. Simulated *full* P116 on a membrane displayed a similar population around ~80° (90° ± 10°), but also a second population around 30° ± 10°, which corresponds to the wringing angle observed in the *refilled* cryo-EM structure (EMD-15276) (Figure 4a, *right*). The ~30° population is directly related to the presence of the cargo and thus, the corresponding conformation is almost never observed for the *empty* P116.

(ii) Arc diameter (Figure 4b): Simulated *empty* P116 in solution and on a membrane displayed an average arc diameter of 11 ± 1 nm, which fits the 11.5 nm arc diameter of the *empty* P116 cryo-EM structure (PDB: 8A9B). Simulated *full* P116 on a membrane displayed a slightly shifted arc diameter population around 12 ± 1 nm, fitting the 12.5 nm arc diameter of the *full* P116 cryo-EM structure (PDB: 8A9A).

(iii) Interdomain angle (Figure 4c): Simulated *empty* P116 in solution and on a membrane displayed an interdomain angle around 90° ± 30° and 100° ± 30°, respectively. Simulated full P116 on a membrane displayed a sharper peak around 90° ± 20°. In general, the observed ranges were much broader than those of the cryo-EM structures, where the interdomain angle lies between 120° and 135°. Interestingly,

the angle is different for each monomer when stably bound to the membrane, i.e. the monomer attached to the membrane has a fixed configuration of the N-terminal domain (Figure 4d), while the N-terminal domain of the solvated monomer is free to move.

The simulated P116 ensemble closely matches the P116 particles in the tomograms (Figure 1a). Inspection of individual particles revealed conformations strikingly similar to those observed in our MD simulations (Figure 4e, Supplemental Figure 7), further corroborating the accuracy of our P116 simulation model.

Overall, the presence of the membrane and the cargo regulate the wringing and interdomain angles accessible by P116 (Figure 4a & d).

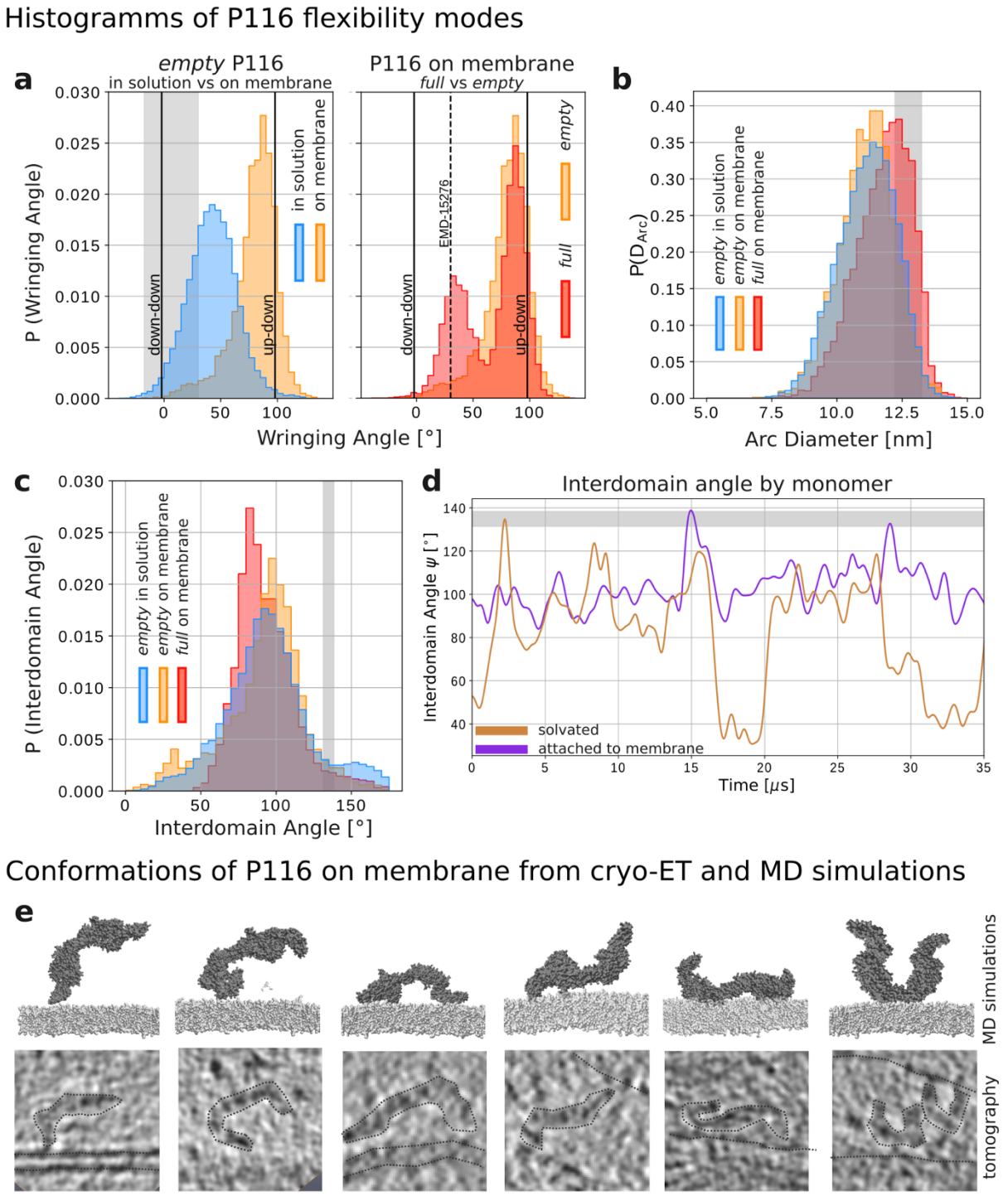

Figure 4: Interaction of P116 with membranes facilitates increased range of motion shown by cryo-ET and MD simulation.

a, b, c Histograms of P116 flexibility modes from MD simulations including empty P116 in solution (blue histograms) and on membrane (orange histograms), and full P116 on membrane (red histograms). Overall, the histograms show a larger flexibility than the range of motion observed in cryo-EM structures of solvated P116 (indicated by grey bars). (a, left) Wringing between monomers was dramatically increased on a membrane, allowing the monomers to face almost opposite directions. Down-down and up-down refer to the directions the central clefts of each monomer are facing. (a, right) The presence of cargo produces two populations of the wringing angle

distribution, in contrast to the empty case, where we observed only one population. The cargo-dependent population at a wringing angle of ~30° corresponds with the wringing angle observed in the cryo-EM structures of *refilled* P116 (EMD-15276, dashed line).
d The interdomain angle between the N-terminal domain and the core domain was consistently at ~135° (grey bars) in cryo-EM structures, while it ranged between 0° and 125° in simulated *empty* P116 on a membrane (in yellow). Stable membrane docking restricted the flexibility range of the attached monomer (in purple).
e Gallery of sub-tomographic projection slices of individual particles (highlighted with dotted lines) in various conformations on the membrane, paired with conformations derived from MD simulations. In all simulation renders, P116 (60–868) is represented by a filled volume in dark grey. The membrane is indicated by the phosphate moiety (represented by silver beads). Water and ions are not shown for clarity.

MD simulations reveal the mechanism of membrane docking

During our membrane simulations, P116 recurrently assumed two membrane-bound conformations (Figure 5a):

(i) 'D-docking': P116 interacted with the membrane using its dorsal side, which contains negative charges that attract lipid head groups (Figure 5a, Supplemental Video 1; Supplemental Figure 10). During the simulations, P116 D-docking modified membrane curvature (Figure 5a).

(ii) 'N-docking': P116 inserted amino acids F860 and F856 into the membrane. The docking was then stabilized through the insertion of F214 and F227 or F87 (Figure 5a & c). Once stabilized, the membrane insertion was maintained for up to 20 µs and placed the DCA right next to the membrane (Figure 5d, Supplemental Video 1). N-docking restricts the interdomain angle of the stably membrane-bound monomer as described in the previous section (Figure 4d). Additionally, this explains why P116 with a truncated N-terminal domain (246–818), which is missing all five membrane-anchoring phenylalanines, could no longer extract lipids from membranes. In all *Mycoplasma* species, residue 214 is a hydrophobic amino acid, while F227 is conserved. In P116, F214 and F227 are part of the N-terminal domain β-sheet, and

F87 is part of an N-terminal domain loop. F856 and F860 are situated on the C-terminal phenylalanine-rich loop (848–868: FAFVDGF) of the core domain, right next to the N-terminal domain (Figure 1b). The C-terminal and N-terminal loops harboring F856, F860 and F87 are part of the hinge domain between N-terminal and core domain.

Chronologically, we always observed that first one monomer associated with the membrane in a D-docking conformation, followed by the N-docking of the other monomer (Figure 5a). This suggests that D-docking plays a role in membrane recognition. The conformation with simultaneous D- and N-docking corresponds to the wringing angle population around 80° in *full* and *empty* P116 (Figure 4a & 5b). The wringing angle population around 30° of *full* P116 corresponds to a conformation that is not stably N-docked to the membrane: none of the phenylalanines on the terminal phenylalanine-rich loop are inserted in the membrane as they are interacting with the cargo (Figure 4a & 5c). The interaction between the phenylalanine-rich loop and the cargo does not allow the DCA to reach the bilayer.

Notably, in the *full* P116 model the pocket does not contain as much cargo as observed in the cryo-EM structures (8A9A and EMD-15276; Figure 4a, Supplemental Figure 8). A larger cargo would enhance the hydrophobicity effect, hence raising the ratio of the 30°-population which is not stably docked to the membrane. Thus, with increasing cargo, the probability for P116 to detach from the membrane is expected to be higher.

The DCA and the membrane are perturbed in N-docking but not in D-docking

Both N-docking and D-docking place the DCA near the membrane (Figure 5d & e). During N-docking, the part of the DCA that can open and close (hereafter referred to as the *gate*) faced the membrane. We repeatedly observed the gate opening (Figure

5d & f). By contrast, during D-docking, the DCA was placed on the membrane with the tip facing down. In addition, the membrane below the docked monomers opened widely during N-docking but not D-docking (Figure 5g).

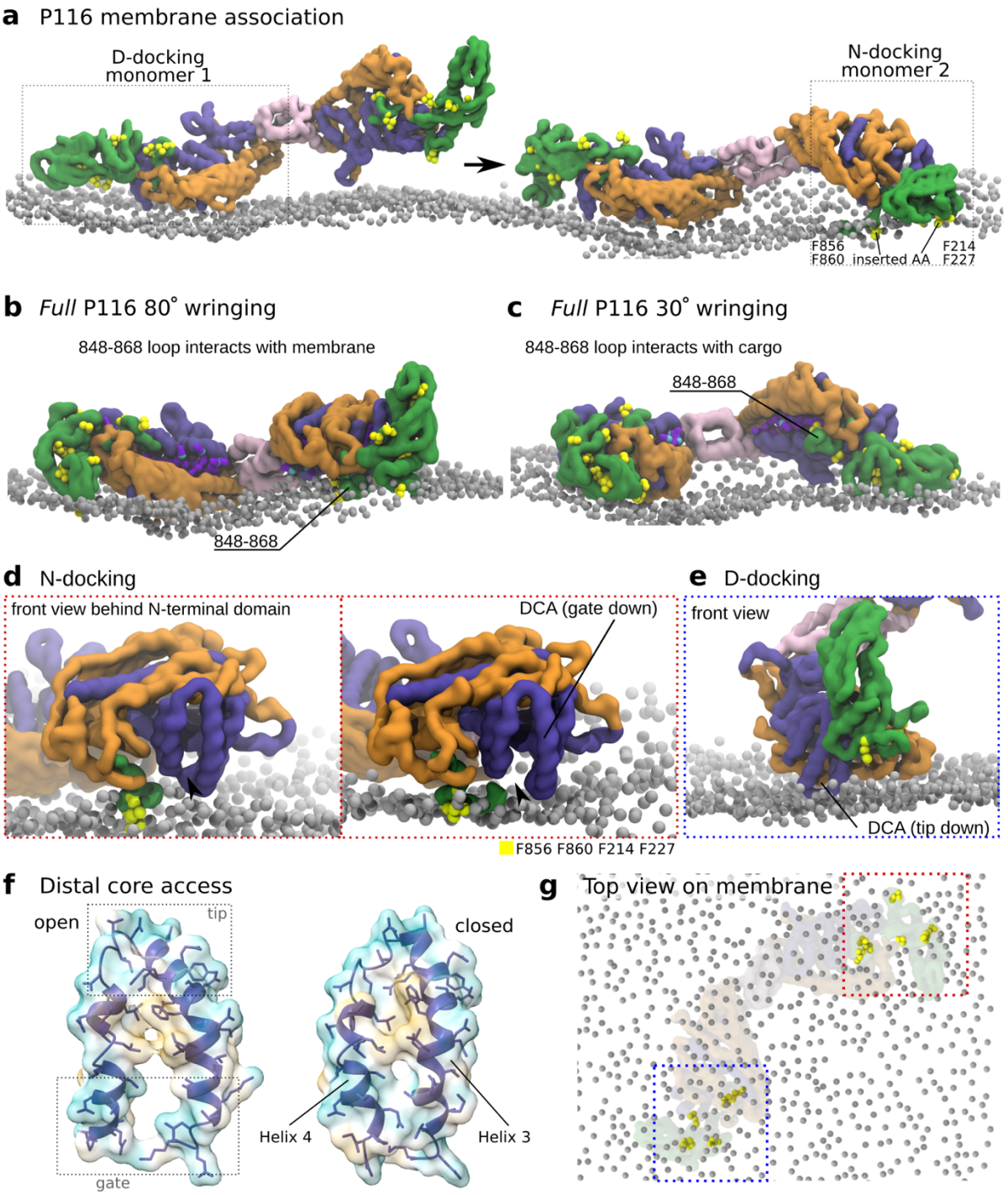

Figure 5: P116 stably docks membranes in MD simulations.
In all simulation renders P116 (60–868) is represented by a filled volume or cartoon representation colored by domain. When present, the membrane is indicated by the

lipid phosphate moieties (represented by silver beads, only one leaflet of the membrane is shown). Water and ions are not shown for clarity.

a Renders from MD simulation of P116. The attachment of P116 to a membrane involves phenylalanine residues (yellow beads) in the N-terminal domain. D-docking of monomer 1 precedes N-docking through insertion of F227 and F214 (shown in yellow) of monomer 2.

b MD simulation of *full* P116 at 80° wringing angle. One monomer is N-docked with the phenylalanine-rich loop (848-868) and F87 inserted in the membrane; and the other monomer is D-docked. All phenylalanine residues on the N-terminal domain are shown as yellow beads.

c MD simulation of *full* P116 at 30° wringing angle. The phenylalanine-rich C-terminal loop (848-868) interacts with the cargo inside the hydrophobic cavity. No phenylalanine residues are inserted stably into the membrane. All phenylalanine residues on the N-terminal domain are shown as yellow beads.

d N-docking places the gate of the DCA near the membrane when closed (left) and opened (right). Residues F860, F856, which insert into the membrane, are shown as yellow beads. The N-terminal domain is not shown.

e D-docking places the tip of the DCA near the membrane. Residues F860, F856 and F87 are shown as yellow beads.

f Details of DCA architecture show opening at the gate side only. Comparison of the DCA conformation between the filled and *empty* cryo-EM structures (PDB: 8A9A and 8A9B, respectively). The two helices comprising the DCA are shown in blue with the individual amino acid sidechains as stick models. The surface representations are colored by hydrophobicity factor (yellow is hydrophobic and blue is hydrophilic). The DCA opens and closes at the gate side while the tip side remains closed.

g N-docking promotes opening of the membrane below the DCA. Top view of the membrane during double docking of P116. The D-docking area is labelled with a blue box, the N-docking area with a red box. Residues F860, F856, F227 and F214 are shown as yellow beads. The membrane barrier is perturbed only during N-docking, which promotes opening of the membrane below the DCA.

IV. The route of lipid uptake and delivery

P116 takes up DOPE lipids via the DCA in simulations

We next investigated the mechanism through which lipids enter P116. We performed an MD simulation of *empty* P116 with free DOPE and DOPG lipids in solution (Figure 6a, *left*). This far-from-equilibrium initial condition enabled us to sample the interactions between P116 and the lipids efficiently. The simulation revealed three events: (i) the formation of micelle-like lipid aggregates; (ii) the interaction of the micelle with the N-terminal domain of the protein and the phenylalanine-rich loop (854–860); (iii) the interaction with the phenylalanine-rich loop and subsequent lipid uptake through the DCA of one monomer. Interestingly, the DCA at the beginning of the simulation was closed (Supplemental Figure 10), and the lipid on the outside of the DCA was caged by F860, F856, F854 and F87 (Figure 6a, *middle*; Supplemental Video 2). Notably, F860 and F856 were inserted into the membrane in the previous simulation (Figure 5a). The lipid uptake was initiated by the flipping of one hydrophobic tail into the DCA followed by the other. The hydrophilic head group remained on the outside of the cavity during the whole process (Figure 6a, *right*, Supplemental Video 2). Once the lipid entered the main cavity, it positioned its head group alternatively towards the central cleft and the dorsal opening. In addition to entering through the DCA into the central cavity, a DOPE molecule also entered the hydrophobic channel of the N-terminal domain, and a lipid micelle stably interacted with the phenylalanine rich loop of the other monomer, further corroborating their involvement in membrane association and lipid binding (Supplemental Video 2). The phenylalanine residues that were inserted during N-docking (F227 and F214) on membrane were involved in binding the lipid within the N-terminal domain.

Next, we investigated how P116 can extract and uptake lipids from membranes. Given that we never observed any spontaneous uptake in the unbiased simulations of the docked P116, we built on the observations of the uptake mechanism of free lipids in solution and judiciously prepared an initial configuration that would facilitate the observation of lipid uptake on membranes. We placed one splayed lipid in the gap between the membrane and the open DCA of the N-docked P116 and ran 48 otherwise unbiased replicas of this system. We observed fast and spontaneous lipid uptake in 40 out of 48 replicas (Figure 6b, Supplemental Figure 9c). We stress that we did not apply any unphysical force to pull the lipid out of the membrane, and after preparing the lipid in a splayed configuration the successive uptake occurred spontaneously. This implies that the lipid splaying is the rate limiting step of this extraction mechanism from membranes.

Both lipid caging and membrane insertion required a high flexibility of the N-terminal domain (Figure 3 and Supplemental Figure 7). When the flexibility was restricted to the range seen in cryo-EM structures, neither N-docking nor placement of lipids at the DCA occurred (Supplemental Figure 9a & b).

Simulation of P116 with cholesterol cargo shows positioning of cholesterol at the DCA

To further study the behavior of the cargo inside the hydrophobic cavity of P116, we performed an atomistic MD simulation of P116 filled with 12 cholesterol molecules per monomer. We used atomistic resolution to optimize for the accuracy of the chemical interactions between cholesterol and the P116 cavity. The amphipathic helices squeezed the cargo into the cavity towards the dimerization domain. This is expected, as the cavity must always be as closed as possible to avoid exposing hydrophobic residues to the solvent. Additionally, this showed that the cavity could

accommodate more than 12 cholesterol molecules, as the simulated volume was smaller as the one observed in the cryo-EM structure of *full* P116 (PDB 8A9A and EMD-15276).

During the simulation, one cholesterol molecule per monomer inserted in the DCA, with the hydroxyl group positioned towards the solvent. Over the course of the simulation, the cholesterol molecules fell back into the cavity, while being replaced by another cholesterol molecule (Figure 6c). This behavior of the cholesterol cargo complements our description of the P116-lipid interactions and show that the delivery and uptake route both go through the DCA.

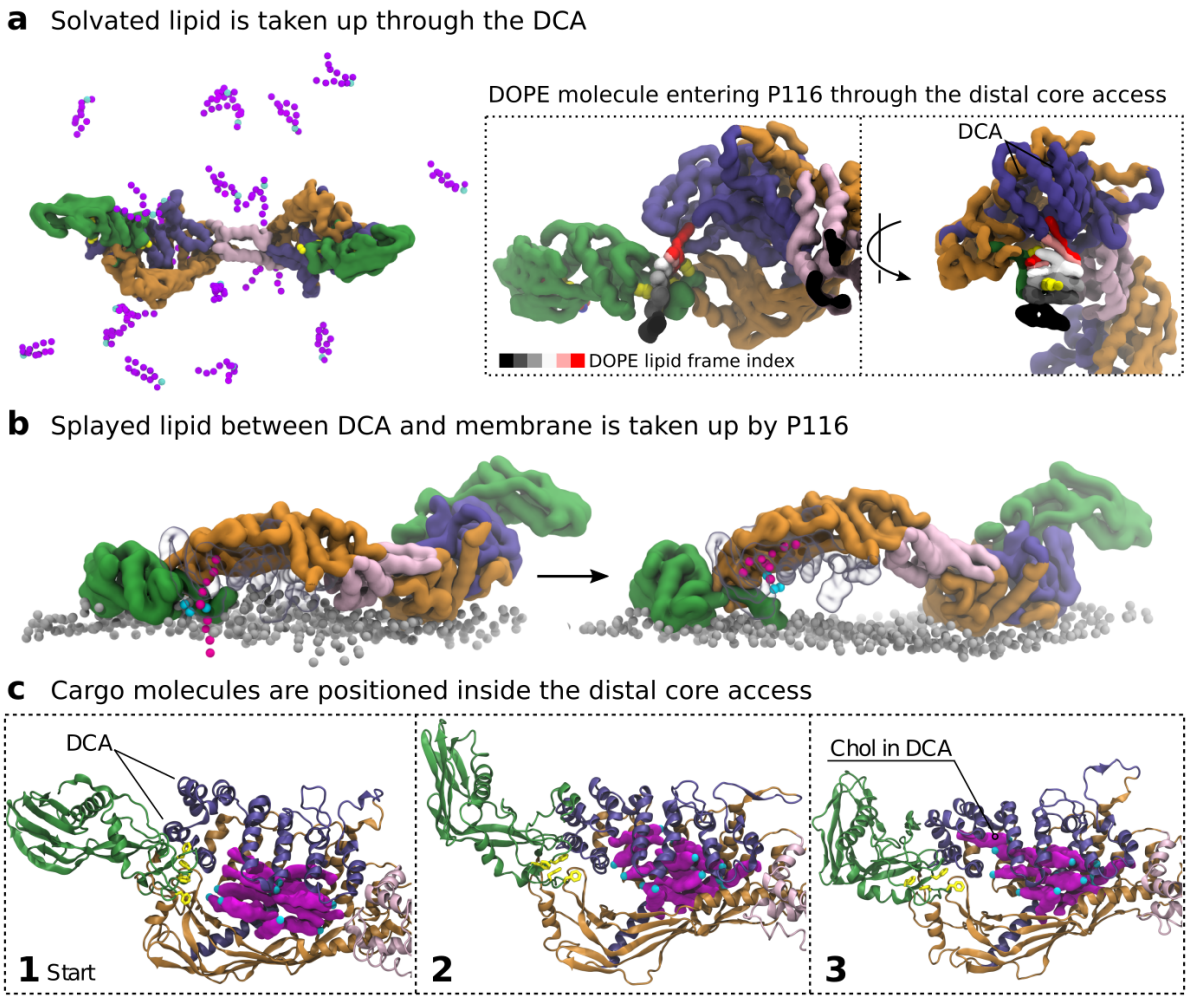

Figure 6: MD simulation reveals mechanism of lipid uptake and delivery by P116. In all simulation renders, P116 is represented by a filled volume or cartoon representation colored by domain. When present, the membrane is indicated by the

phosphate moiety (silver beads) and solvated lipids are represented by phosphate moieties (blue beads) and tails (purple beads). Water and ions are not shown for clarity.
a Solvated lipids enter P116 through the DCA. Coarse-grained MD simulation of P116 with free-floating DOPE, DOPC and DOPG lipids. F860, F856, F227 and F214 are shown as yellow beads. (Left) Start of simulation with evenly distributed lipids. (Right) DOPE lipid entering the cavity through the DCA. The lipid is shown as a filled volume colored according to the trajectory frame.
b Lipids are taken up by P116 when placed in a splayed configuration between the membrane and DCA. (Left) N-docked P116 with a splayed DOPE lipid positioned below the DCA. (Right) DOPE lipid entering the cavity through the DCA. The DCA and amphipathic helices of the N-docked monomer are rendered as transparent shapes for clarity.
c Cargo inside the cavity is positioned inside the DCA. Atomistic MD simulation of 12 cholesterol molecules (shown as purple spheres) in the cavity of P116. $\mathbf{c_1}$ Start of simulation with cholesterol molecules evenly distributed inside the cavity. $\mathbf{c_2}$ Cholesterol molecules rearrange and are squeezed into the cavity towards the dimerization domain. $\mathbf{c_3}$ An individual cholesterol molecule inserts in the hydrophobic channel formed by the DCA.

Discussion

Mycoplasma evolved an integrated lipid transport system composed of a single protein, P116, that can self-sufficiently acquire and deliver lipids. Our data showed that the mechanism is based on two docking modes: (i) N-docking enables stable association with the membrane through insertion of phenylalanine residues (Figure 5a). (ii) D-docking helps to modulate lipid transfer directionality through interactions between the negatively charged dorsal interface and the membrane (Supplemental Figure 10). The membrane of mycoplasma contains approximately 30% anionic lipids, whereas the outer leaflet of eukaryotic cells is neutral and contains mostly cholesterol, PC and SM[14,15]. As a result, D-docking should be favored on the host cell membrane. This is corroborated by the fact that P116 faces high-density lipoprotein particles with its dorsal side[6]. In our simulations, D-docking of one monomer through long-range

electrostatic interactions brought the second monomer close enough to the membrane to allow for N-docking. Lipids are then taken up by the N-docked monomer (Figure 6b and Supplemental Video 2).

Lipid transfer by P116 happens without the consumption of ATP, thus, the lipid concentration gradient must drive uptake and delivery. The lipids will slide towards the hydrophobic core that exerts the largest force: towards the cavity when the pocket is empty and towards the membrane when the pocket is filled, in both instances to equilibrate the lipid concentration. After docking to a membrane, the cavity of the N-docked monomer is filled with host membrane lipids. Consequently, the lipid composition gradient is equilibrated, and lipid uptake is interrupted. At this point, the larger the amount of the cargo, the more likely the phenylalanine rich loop is to interact with it. Such interaction makes N-docking impossible, thus P116 is not stably bound to the membrane and more likely to detach (Figure 7). This provides P116 the opportunity for either lipid uptake of the other monomer from the host, or delivery to *Mycoplasma* because of the different lipid composition. Due to the electronegativity of the bacterial membrane and the lipid composition gradient, we expect the N-docking of the other monomer to be favored. Once the amount of cargo in the cavities is large enough, N-docking is hindered and docking to the host is energetically disfavored. Instead, docking to *Mycoplasma* is incentivized by the presence of the membrane linker (purple in Figure 7), which stochastically increases the opportunity for membrane association.

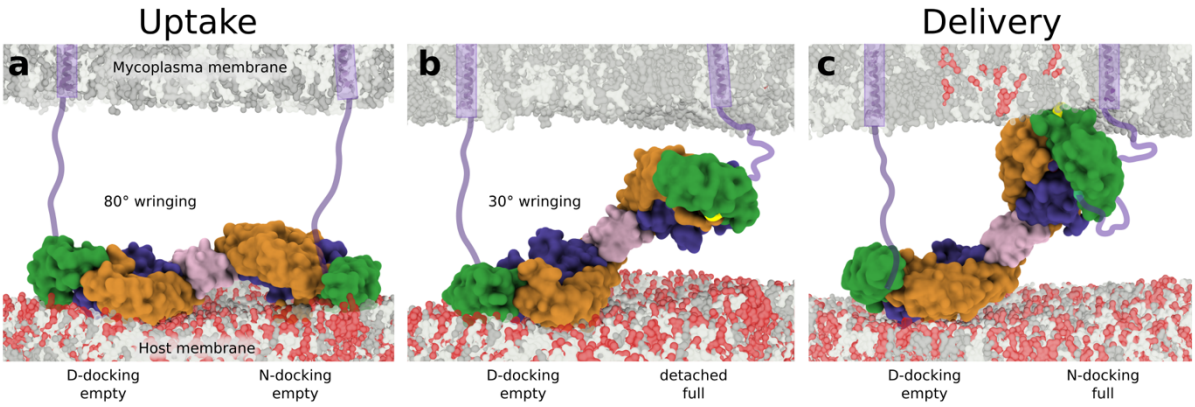

Figure 7: Cartoon of uptake and delivery mechanism in P116.
a When empty, P116 is flexible enough to D-dock one monomer while N-docking the second monomer. The D-docking happens first, as it is based on long-range electrostatic interactions, and brings the second monomer close to the membrane to insert several phenylalanine residues (N-docking). Lipids then enter P116 through the DCA.
b After the second monomer is filled, interaction of the phenylalanine residues with the cargo causes the N-docked monomer to detach from the host membrane.
c The filled monomer can now dock to the mycoplasma membrane and deliver its lipids through the DCA, driven by the lipid concentration gradient. Docking to the Mycoplasma membrane is more probable through the membrane linker.

What determines the transfer directionality of P116, i.e. uptake from the host and delivery into the mycoplasma membrane and not the opposite? Differently than other LTPs, such as Osh4p, for which the membrane affinity depends on the specific type of cargo[16], P116 can bind a broad range of lipids, including lipids that are not essential for *Mycoplasma*. Ultimately, the net transfer of lipids is due to the different concentration of lipids in the host and pathogen membranes in combination with P116's architecture. Unlike in SMP domains[2], the membrane-sensitive residues of P116 (dorsal interface) are not adjacent to the membrane binding interface, and whether both interfaces preferably face the membrane simultaneously depends on the filling state of the protein (Figure 4a, *right*). This interdependency between the filling state and protein flexibility effectively results in a cargo-volume-dependent membrane affinity. This exceptional feature of P116, when compared to other LTPs, is enabled by

its unique structure. Lipids are not stored within the LTP module, e.g. the SMP-like N-terminal domain; instead, P116 evolved an outstandingly large core domain that can bind varying amounts of cargo. Such a mechanism of transfer directionality dependent on the amount of cargo within a putative LTP has never been described before. In this sense, our insights into the lipid acquisition mechanism in *M. pneumoniae* advance the understanding of lipid transport pathways in other bacteria and eukaryotes.

Material & Methods

Overexpression of native P116 in *M. pneumoniae*

The gene *mpn213* (coding for P116) was amplified from isolated genomic DNA of *M. pneumoniae* strain M129 using primers 5' CAGGACTCGAGCCGTTTGTTTAAGGACAA-AAC 3' and 5' GGAGATATCCTAAAAACCAACGAACCAGAAG 3', bearing an EcoRV and a XhoI restriction site, respectively. As little is known about Mycoplasma promoters and enhancers, the position of the forward primer was chosen at the end of *mpn212*, upstream of *mpn213*, to include the native promoter and regulatory elements. The *M. pneumoniae* replicating plasmid pGP2756[17], was linearized by PCR using primers 5' CTGAGATATCTAGTTATTG-CTCAGCGGTGG 3' and 5' CAGGACTCGAGCACTTTTCGGGGAAATGTGC 3', bearing an EcoRV and a XhoI restriction site, respectively. After restriction with the respective enzymes, the linearized backbone and amplified gene were ligated and used to transform DH5α *Escherichia coli* cells. The resulting plasmid is available upon request.

After verification by sequencing, *M. pneumoniae* cells were transformed as previously described[18]: *M. pneumoniae* cultures were grown to late-exponential phase in 75 cm^2 culture flasks. The adherent cell layer was washed three times with chilled electroporation buffer (8.0 mM HEPES, 272 mM sucrose, pH 7.4), scraped off and resuspended in 0.5 mL of the same buffer. The suspension was passed ten times though a 25-gauge syringe needle. Then, 200 µL aliquots were mixed with 1 µg of the plasmid and transferred to 0.2 cm electro cuvettes (BIO-RAD, Hercules, USA), chilled for 15 min on ice, and electroporated in a BIO-RAD MicroPulser Electroporator using the Ec2 preset (2500 V). After pulsing, the cells were chilled on ice for 15 min before 600 µL of prewarmed SP4 medium was added. Cells were allowed to recover at 37°C

for 2 h before the transformation volume was inoculated into a 75 cm^2 tissue culture flask filled with 20 mL medium containing 10 µg/mL tetracycline and further cultured at 37°C.

Expression and purification of P116

The extracellular domain of P116, C-terminally shortened and HIS-tagged (30–957), was expressed via the vector pOPINE_P116 backbone #26043; Addgene, Watertown, USA). The vector is available upon request. *E. coli* BL21 (DE3) cells harboring the vector were grown at 37°C to an OD_{600} of 0.6, induced with 0.6 mM IPTG and further grown overnight at 20°C with mild shaking. Cells were harvested, lysed by sonication in lysis buffer (50 mM Tris-HCl, pH 7.4, 20 mM imidazole, 1 mM PMSF) and centrifuged at 20,000 x g in a tabletop centrifuge for 45 min at 4°C. The supernatant was loaded onto a HisTrap 5 mL column (GE Healthcare, Chicago, USA) that was pre-equilibrated in binding buffer (20 mM Tris-HCl, pH 7.4, 20 mM imidazole), thoroughly washed in binding buffer and eluted with elution buffer (20 mM Tris-HCl pH 7.4, 400 mM imidazole, 150 mM NaCl). The eluate was loaded onto a Superose 6 column (GE Healthcare, Chicago, USA) in protein buffer (20 mM TRIS-HCl, pH 7.4, 150 mM NaCl). Fractions containing non-aggregated P116 were pooled and stored at –80 °C.

Emptying of P116

To obtain *empty* P116, we added 2.6% Triton X-100 to the protein sample and incubated it for either 1.5 h at room temperature (full-length P116) or 3 h at 37°C (construct without the N-terminal domain) with shaking. The Triton X-100 was then removed by either (i) binding to a HisTrap 1 mL column (GE Healthcare, Chicago, USA) or HIS-Select Nickel Affinity Gel in a gravity-flow column (Merck, Darmstadt, Germany), followed by washing with binding buffer with and without 1.3% Triton X-100, before

eluting the samples from the column; or (ii) diluting twice to 15 mL and then to 95% concentration in a centrifugal concentrator (Pierce, 50,000 MWCO PES; Thermo Fischer Scientific, Waltham, USA) and subsequently running through a detergent removal spin column (Pierce; Thermo Fischer Scientific, Waltham, USA). P116 was concentrated using Vivaspin 500 centrifugal concentrators (10,000 MWCO PES; Sartorius, Göttingen, Germany) to a final concentration of >0.5 mg/mL.

Preparation of liposomes

Generally, lipids were dissolved in chloroform, then mixed and dried under nitrogen followed by high vacuum overnight. The dried lipid mixtures were then slowly dispersed in liposome buffer (20 mM Tris-HCl, pH 7.4) and left to hydrate for 30 min with gentle agitation. The liposomes were extruded with an Avanti Mini-Extruder (Avanti Polar Lipids, Alabaster, USA) and stored at 4°C in the dark.

Fluorescent liposomes (30% Dansyl-DOPE, 30% NBD-DOPC and 40% DOPG) were prepared from 1 mg of Dansyl-DOPE, 0.75 mg NBD-DOPC and 1 mg DOPG, respectively (Avanti Polar Lipids #810330c, #810132c and #840475c, respectively). Hydration and extrusion were performed at room temperature to a final concentration of 2.75 mg/mL and a diameter of 200 nm. DPPC and SM liposomes were prepared with the pure lipids (Avanti Polar Lipids DPPC #850355c, Egg-SM #860061c, respectively). Hydration was carried out at 50°C and 60°C, respectively, to a final concentration of 3 mg/mL. The liposomes were not extruded.

Cargo binding assay

Previously emptied P116 was incubated with an excess of DPPC liposomes in buffer. The incubation was carried out in 50 µL total volume for 2 h at 37°C with mild shaking. The liposomes were removed by ultracentrifugation for 30 min at 150,000 x g

in a Ti70 rotor with 1.5 mL Eppendorf tube adapters and re-ultracentrifugation of the upper 80% of supernatant, before collecting the upper 90% of supernatant and washing it three times in 50,000 MWCO centrifugal concentrators (Vivaspin 500, PES; Sartorius, Göttingen, Germany). Efficient removal was verified by MALDI-TOF mass spectrometry. Unspecific binding of DPPC to the filter or tube wall was tested by repeating the procedure detailed above. Binding of compounds to P116 via unspecific protein effects was tested by repeating the procedure detailed above in the presence of P110 and P140, *M. pneumoniae* membrane proteins.

Lipid transfer assay

To fill P116 with fluorescent lipids, 0.5 mg of emptied P116 was incubated with 50 µL of freshly extruded fluorescent donor liposomes (30% Dansyl-DOPE, 30% NBD-DOPC, 40% DOPG) for 2 h at 37°C with gentle shaking.

The fluorescent liposomes were then removed by ultracentrifugation for 30 min at 150,000 x g in a Ti70 rotor with 1.5 mL Eppendorf tube adapters and re-ultracentrifugation of the upper 80% of supernatant, before collecting the upper 90% of supernatant. Efficient removal was verified by MALDI-TOF mass spectrometry. The supernatant was concentrated using 10,000 MWCO centrifugal concentrators (Vivaspin 500, PES; Sartorius, Göttingen, Germany) to a volume <100 µL. It is important that the liposome-protein solution is re-suspended well by pipetting up and down before ultracentrifugation.

DPPC acceptor liposomes were prepared by 5x ultrafiltration in a 0.2 µm centrifugal concentrator (Vivaspin 500, PES; Sartorius) at 6,000 x g and dilution with liposome buffer. This eliminates smaller liposomes that would be lost in subsequent steps and cannot be imaged by the laser scanning microscope with a 63x/1.4 oil objective. Thorough re-suspension between rounds is crucial.

P116 filled with fluorescent lipids was incubated with DPPC acceptor liposomes for 2 h at room temperature with gentle shaking. P116 was then removed by washing four times with liposome buffer via ultrafiltration in 300,000 MWCO centrifugal concentrator (Vivaspin 500, PES) at 6,000 x g. The process was monitored by measuring the P116 concentration in the flow-through until total protein is recovered and the concentration in the filtrate is zero. A dot blot was used to verify that the concentration of P116 in the filtrate was << 0.5 µg. The resulting sample was subjected to analysis by MALDI-TOF mass spectrometry and laser-scanning microscopy. To account for spontaneous insertion of fluorescent lipids into the acceptor liposomes or spontaneous fusion between acceptor and donor liposomes from possible donor liposome contaminations of the final sample, the procedure detailed above was repeated in the absence of P116, and the sample was subjected to analysis by laser-scanning microscopy. All experiments were carried out in triplicate, and all results could be replicated.

HaCaT cells were grown in DMEM with 10% FCS, thinly seeded in 8-well plates (ibidi, Gräfelfing, Germany) and allowed to adhere overnight. P116 filled with fluorescent lipids was added to the cells in serum-free DMEM and incubated for 30 min at 37°C. The cells were then washed three times with DMEM and left to recover for 2 h at 37°C in DMEM with 10% FCS.

Laser scanning microscopy

Laser-scanning fluorescence microscopy was performed on an inverse confocal microscope (LSM780, Axio Observer Z.1; Carl Zeiss, Jena, Germany) with a Plan-Aptochromat 63x/1.4 oil objective and Immersol 518F (Carl Zeiss, Jena, Germany) using laser lines at 405 nm and 458 nm. The pinhole was set to 1 airy unit. Imaging was done in an 8 µL drop of sample in an 8-well µ-Slide with glass bottom (ibidi). The

fluorescence intensity of individual liposomes was analyzed with Zeiss ZEN 2012 (black) v.8.0.5.273 and ImageJ 1.53t[19].

Matrix-assisted laser desorption/ionization mass spectrometry

All samples were mixed in a 1:1 ratio with sDHB (Super-DHB; Bruker, Billerica, USA) matrix solution (50 mg mL in 50% acetonitrile (ACN), 50% water, and 0.1% trifluoroacetic acid). Subsequently, 1 µL aliquots of the mixture were deposited on a BigAnchor MALDI target (Bruker, Billerica, USA) and allowed to dry and crystallize at ambient conditions. MS spectra were acquired on a rapifleX MALDI-TOF/TOF (Bruker, Billerica, USA) in the mass range of 100–2,000 m/z in reflector positive and negative mode for lipid measurements. The Compass 2.0 (Bruker, Billerica, USA) software suite was used for spectra acquisition and processing.

Single-particle cryo-EM

A 3.5 µL drop of purified P116 (300 µg/mL in 20 mM Tris, pH 7.4 buffer for peptide-filled P116 (30–957) and 3 mg/mL in 20 mM Tris, 0.5 mM CHAPSO, pH 7.4 buffer for P116 without the N-terminal domain (246–818)) was applied to a 45 s glow-discharged R1.2/1.3 C-flat grid (Electron Microscopy Science, Hatfield, USA), and plunge-frozen in liquid ethane (Vitrobot Mark IV; Thermo Fischer Scientific) at 100% relative humidity, 4°C, a nominal blot force of –3, a wait time of 0.5 s, and a blotting time of 12 s. Before freezing, Whatman 595 filter papers were incubated for 1 h in the Vitrobot chamber at 100% relative humidity and 4°C.

Dose-fractionated movies of P116 (246–818) were collected with SerialEM v4.1.0beta[20] at a nominal magnification of 165,000 (0.819Å per pixel) in nanoprobe EFTEM mode at 300 kV with a Titan Krios (Thermo Fischer Scientific) electron microscope equipped with a GIF Quantum S.E. post-column energy filter in zero-loss

peak mode and a K2 Summit detector (Gatan, Pleasanton, USA). A total of 4,314 micrographs with 50 frames per micrograph and a frame time of 0.1 s were collected. The camera was operated in dose-fractionation counting mode with a dose rate of ~8 electrons per $Å^2$ s^{-1}, resulting in a total dose of 60 electrons per $Å^2$. Defocus values ranged from –1 to –3.5 µm.

For emptied and *refilled* P116 (246–818), dose-fractionated movies were collected using EPU v.3.1.3 (Thermo Fischer Scientific) at a nominal magnification of 105,000 (0.837 Å/pix) in nanoprobe EFTEM mode at 300 kV with a Titan Krios G3i electron microscope (Thermo Scientific) equipped with a BioQuantum-K3 imaging filter (Gatan) and operated in zero-loss peak mode with 30 eV energy slit width. In total, 8,002 micrographs with 50 frames per micrograph and a frame time of 0.05 s were collected. The K3 camera was operated in counting mode with a dose rate of ~15 electrons per $Å^2s^{-1}$, resulting in a total dose of 50 electrons per $Å^2$. Defocus values ranged from –0.8 to –3.5.

CryoSPARC v3.2[21] was used to process the cryo-EM data, unless stated otherwise. Beam-induced motion correction and contrast transfer function (CTF) estimation were performed using CryoSPARC's own implementation. For the dimers P116 (246–818), particles were initially clicked with the Blob picker using a particle diameter of 200–300Å. Particles were then subjected to unsupervised 2D classification. For the final processing, the generated 2D averages were taken as templates for the automated particle picking. In total, 1,197,649 particles were picked and extracted with a binned box size of 256 pixels. False-positive picks were removed by two rounds of unsupervised 2D classification. The dimerization rate of the core construct (246–818) was substantially less than that of the whole ectodomain (30–957), as evidenced by the presence of approximately 50% monomers in the 2D classes of the purified protein and >90% monomers in the 2D classes of the protein after

emptying and refilling, compared with only dimers in the 2D class averages of the full-length ectodomain. The remaining 225,218 particles were used to generate an *ab initio* reconstruction with three classes followed by a heterogeneous refinement with three classes. For the final processing, 101,747 particles were used. For the remaining particles, the beam-induced specimen movement was corrected locally. The CTF was refined per group on the fly within the non-uniform refinement[22]. The obtained global resolution of the homodimer was 4.3 Å (Supplemental Figure 3). For truncated P116 (246–818) after attempted refilling, particles were initially clicked with the Blob picker using a particle diameter of 100–200 Å. Particles were then subjected to unsupervised 2D classification. For the final processing, the generated 2D averages were taken as templates for the automated particle picking. In total, 6,997,649 particles were picked for the monomer and 1,650,962 particles for the dimer, and extracted with a box size of 256 pixels. False-positive picks were removed by two rounds of unsupervised 2D classification. The remaining 1,470,056 particles for the monomer and 446,980 particles for the dimer, were used to generate an *ab initio* reconstruction with three classes followed by a heterogeneous refinement with three classes. For the final processing, 518,561 particles were used for the monomer and 145,945 particles for the dimer. For the remaining particles, the beam-induced specimen movement was corrected locally. The CTF was refined per group on the fly within the non-uniform refinement[22]. As initial volumes for the non-uniform refinement, maps were built with residues 246–818 from PDB: 8A9A (filled P116) and PDB:8A9B (empty P116) and filtered to 30 Å. Both maps yielded similar refined structures. The obtained global resolution was 5.43 Å for the monomer and 6.52 Å for the dimer (Supplemental Figure 3).

Cryo-electron tomography of *M. pneumoniae*

Adherently growing *M. pneumoniae* cells overexpressing P116 were harvested by scraping 2 days after transformation without washing, and pelleting for 20 min at 15,000 x g. The pellet was washed once in 1 mL PBS, re-pelleted and then resuspended in 100 µL PBS. Multiple dilutions of the suspension were prepared and passed multiple times though a 25-gauge syringe needle until all clumps were resolved. The solution was mixed with fiducial markers (Protein A conjugated to 5 nm colloidal gold; Cell Biology Department, University Medical Center Utrecht, The Netherlands) in some cases. From the solutions with or without fiducials, a 3.5 µL drop was applied to a (45 s) glow-discharged R1.2/1.3 C-flat grid (Electron Microscopy Science, Hatfield, USA) with a 4 nm carbon coat, and plunge-frozen in liquid ethane (Vitrobot Mark IV; Thermo Fischer Scientific) at 100% relative humidity, 4°C, and a nominal blot force of –1, with wait and blotting times of 8–12 s.

Tilt-series were recorded using SerialEM v4.0.14[20] at a nominal magnification of 81,000 (1.112 Å per pixel) in nanoprobe EFTEM mode at 300 kV with a Titan Krios G2 (Thermo Fischer Scientific) electron microscope equipped with a BioQuantum-K3 imaging filter (Gatan), operated in zero-loss peak mode with 20 eV energy slit width, and a K3 Summit detector (Gatan). The total dose per tomogram was 120 $e^{-}/Å^{2}$, and the tilt series covered an angular range from −60° to 60° with an angular increment of 3° and a defocus set at −3 µm. Local motion correction and CTF estimation of tilt series were done in Warp v.1.0.9[23]. Image stack alignment was done in IMOD v.4.11.8.[24] Tomograms were reconstructed in Warp v.1.0.9. Particles were clicked on deconvoluted tomograms in ArtiaX v1.0 (ChimeraX extension)[25]. Sub-tomograms were reconstructed with Warp, using the star files from ArtiaX after adding micrograph names and modifying the header. Initial models from sub-tomograms and 3D refinement were done with Relion v.3.1[26] with 698 homogenous and 1101

heterogeneous particles, a box size of 128 pixels, a pixel size of 4.445 Å/pix, a mask diameter of 450 Å, and a resolution of ~30 Å (EMD-18629). Filtered and projected sub-tomograms of individual particles were inspected in Amira v.5.3.3 (Thermo Fischer Scientific).

Molecular dynamics simulations

Coarse-grained *empty* P116 dimer on membrane. First, we generated the MARTINI coarse-grained P116 dimer on a symmetrical bilayer membrane (30% DOPC, 30% DOPE, 40% DOPG) using the Charmm-GUI MARTINI maker webserver (bilayer builder) with the MARTINI 3.0 forcefield[34–36] on the PDB structure 8A9A (UniProt serial numbering, residues 60–868 per chain). We prepared two different models. One retained all the *interdomain* elastic network (EN) generated by the software (via martinize2) to keep the N-terminal domain fixed as seen in the cryo-EM structures (PDB 8A9A 8A9B) (model **Restrained empty on membrane** in Table 1). For the second model (model **Empty on membrane** in Table 1), we modified the EN to retain only *intradomain* bonds (we later used this criterion for all the CG simulations except otherwise stated). Additionally, we prepared another model where we included the C-terminal stretch of about 100 amino acids to obtain the P116 60-957 model as used in the biophysical assays (model **Empty with C-terminus** in Table 1). To do so, in absence of an experimental structure, we used the AlphaFold Colab[37] prediction of the C-terminal stretch (UniProt serial numbering 868-957 per chain). We merged the P116 60-868 model to two copies of the predicted structure using USCF Chimera[27]. We modified the EN of this model to retain only the *intradomain* bonds.

For each model, using GROMACS 2021.4, we ran a 5000-step soft core (*free-energy* = *yes*) minimization followed by a 3000-step hard core (*free-energy* = *no*) minimization, both using the steepest descent algorithm. Then, we ran six rounds of

NPT equilibration per system at a reference temperature of 310 K (V-rescale thermostat, τt = 1 ps) and a reference pressure of 1 bar (Berendsen barostat, semi-isotropic coupling type, τp = 5 ps[38]) with ever-decreasing force constant on the position restraints of the membrane. We then simulated the systems in NPT ensemble using GROMACS 2021.4 with 0.15 M NaCl at a reference temperature of 310 K (V-rescale thermostat, τt = 1 ps) and a reference pressure of 1 bar (Parrinello-Rahman barostat, semi-isotropic coupling type, τp = 5 ps). We used a time step of 20 fs. To avoid unphysical behavior in the equilibrated P116 60-957 we firstly enabled the hydrophobic pockets to collapse while keeping the 868-957 loop restrained in place.

The comparison of the simulated dynamical ensembles with the tomograms of *M. pneumoniae* revealed the incompatibility of the P116 60-868 with *interdomain* EN and P116 60-957 ensembles (see Supplemental Figure 7c & d), while P116 60-868 without interdomain EN showed a remarkable agreement (see Figure 4b and Supplemental Figure 7c &d). We thus chose the P116 60-868 model without interdomain EN for the MD simulations as it is predictive of the P116 dynamics.

The simulation of P116 60-868 showed docking of the protein to the membrane. We took a docked configuration obtained with the previous run and used it to reinitialize the system where three lipids in proximity of the DCA of the docked P116 monomer were pulled towards the DCA using UCSF Chimera[27] (model **Empty with pulled lipids** in Table 1). This was a first attempt to favor the lipid uptake. The new input model was solvated using the *insane.py* script[39]. We used a NaCl concentration of 0.15 M with neutralizing ions. We ran a 5000-step minimization using the steepest descent algorithm. Then, we ran an NPT equilibration at a reference temperature of 310 K (V-rescale thermostat, τt = 1 ps) and a reference pressure of 1 bar (Berendsen barostat, semi-isotropic coupling type, τp = 5 ps). We simulated this system in NPT ensemble using GROMACS 2021.4 at a reference temperature of 310 K (V-rescale thermostat,

τt = 1 ps) and a reference pressure of 1 bar (Parrinello-Rahman barostat, semi-isotropic coupling type, τp = 5 ps) for about 35 μs. Coulombic interactions were treated with PME and a cut-off of 1.1 nm as for van der Waals interactions. We used a time step of 20 fs. During this simulation, P116 steadily docked to the membrane via residues F214 and F227 (see Figure 5a).

Coarse-grained *empty* P116 dimer on membrane with one splayed lipid tail. Based on a frame from the simulation of the *empty* P116 dimer steadily N-docked on the membrane, we created a model where one lipid tail was splayed to be in between the DCA helices and the other tail was inserted in the membrane bilayer. One lipid was deleted from the previous model to allow the positioning of the splayed lipid using UCSF Chimera[27] (model **Empty docked with splayed lipid** in Table 1). The new input model was solvated using the *insane.py* script[39]. We used a NaCl concentration of 0.15 M with neutralizing ions. We ran a 5000-step minimization using the steepest descent algorithm. Then, we ran an NPT equilibration at a reference temperature of 310 K (V-rescale thermostat, τt = 1 ps) and a reference pressure of 1 bar (Berendsen barostat, semi-isotropic coupling type, τp = 5 ps). We simulated this system in NPT ensemble using GROMACS 2021.4 at a reference temperature of 310 K (V-rescale thermostat, τt = 1 ps) and a reference pressure of 1 bar (Parrinello-Rahman barostat, semi-isotropic coupling type, τp = 5 ps). Coulombic interactions were treated with PME and a cut-off of 1.1 nm, as for van der Waals interactions. We used a time step of 20 fs. We ran 49 replicas of this system which resulted in 41 replicas extracting the lipid and 8 where the lipid did not move or escaped. We computed the statistics based on a 1 nm distance threshold between the lipid and the cavity inner dorsal side.

Coarse-grained *full* P116 dimer on membrane. Using the same procedure used for the *empty* P116 we obtained the *martinized* model of PDB 8A9A (UniProt serial numbering, residues 60–868 per chain). We proceeded to fill the hydrophobic pockets with lipids (2 DOPCs, 1 DOPEs, 6 DOPGs per pocket) using UCSF Chimera[27] (model **Full on membrane** in Table 1). We solvated the model using the *insane.py* script[39]. We maintained the parameters and equilibration protocol consistent with those used for the *empty* P116 model on membrane but used GROMACS 2022.4 for equilibration and production runs.

Coarse-grained *empty* P116 dimer in solution with DOPG, DOPE and DOPC lipids. Using the topology of the P116 dimer and lipids from the simulations with membrane and the equilibrated P116 dimer configuration, we created the model of the P116 dimer with sealed hydrophobic pockets surrounded by 15 DOPGs, 7 DOPCs and 7 DOPEs using UCSF Chimera[27]. We prepared two models: one with *interdomain* EL (model **Restrained empty in solution** in Table 1) and one retaining only *intradomain* EL bonds (model **Empty in solution** in Table 1). We then used the *insane.py* script[39] to solvate the systems. We used a NaCl concentration of 0.15 M with neutralizing ions. Using GROMACS 2021.4, we ran a 5000-step minimization using the steepest descent algorithm and ran an NPT equilibration at a reference temperature of 310 K (V-rescale thermostat, τt = 1 ps) and a reference pressure of 1 bar (Berendsen barostat, semi-isotropic coupling type, τp = 5 ps), for each system. We simulated the systems in the NPT ensemble using GROMACS 2021.4 with 0.15 M NaCl concentration at a reference temperature of 310 K (V-rescale, τt = 1 ps) and a reference pressure of 1 bar (Parrinello-Rahman barostat, isotropic coupling type, τp = 12 ps). Coulombic interactions were treated with PME and a cut-off of 1.1 nm, as for van der Waals interactions. We used a time step of 20 fs.

Definition of arc diameter, wringing angle, the interdomain angle and reference structures. We defined the *arc diameter* of P116 as the average of the distances between residues 416 of chain A and 253 of chain B and between residues 253 of chain A and 416 of chain B per frame.

We defined the *wringing angle* as the angle between the planes containing the centers of mass of residues 280 and 301 and of the whole core domain of each monomer. We defined as offset the wringing angle achieved when the two monomers were both facing approximately downwards (in general, in the same direction). We then subtracted this value from the raw values to set the *down-down conformation* at $\sim 0°$. Accordingly, we find that the *up-down conformation* is at $\sim 100°$.

We defined the *interdomain angle* as the angle between the segments connecting the centers of mass of

- the residue pairs 164 and 181, and 107 and 108 and
- the residue pair 382 and 404 and the group 708 to 712.

We defined as *reference structures* the MARTINI CG models of the cryo-EM structures (*full* P116 with PDB 8A9A, *empty* P116 with PDB 8A9B and *refilled* P116 EMD-15276). For this purpose, we did not modify the elastic network of the model, to keep the conformation as close as possible to the cryo-EM structure except for the open pocket. All reported values are the mean (for the wringing angle and the arc) or the median (for the interdomain angle) $\pm$ the one standard deviation of the distributions.

Atomistic simulation of the P116 dimer filled with cholesterol. We created an atomistic model of the P116 dimer (UniProt serial numbering, residues 60–868 per monomer) with each hydrophobic pocket filled with 12 cholesterols using UCSF Chimera[27] (model **Full with Cholesterol** in Table 1). We solvated the system with

TIP3P water using GROMACS[28]. We minimized the system using the steepest-descent algorithm for 5000 steps and performed a 200-ps-long NVT equilibration using the V-rescale thermostat[29] with a reference temperature of 310 K (τt = 0.1 ps). We simulated the system in the NPT ensemble for 0.6 μs using the Charmm36m forcefield[30–32], a reference temperature of 310 K (τt = 1 ps, V-rescale thermostat), a reference pressure of 1 bar (τp = 5 ps, Parrinello-Rahman barostat[33]) and a NaCl concentration of 0.15 M. For both the van der Waals (Verlet) and the Coulomb forces (Particle Mesh Ewald), we used a $r_{\mathrm{cut-off}} = 1.2\ \mathrm{nm}$. We chose a 2 fs time step. We used GROMACS 2021.4.

Table 1: Models used for MD simulations, simulated time and number of runs

MODEL	SIMULATED TIME	N° RUNS
Full with Cholesterol	0.6 μs	1
Empty on membrane	33 μs	1
Restrained empty on membrane	21 μs	1
Empty with pulled lipids	35 μs	1
Empty in solution	22 μs	1
Restrained empty in solution	4 μs	1
Empty docked with splayed lipid	14 μs	49
Full on membrane	36 μs	1
Empty with C-terminus	14 μs	4

Data Availability

The cryo-EM structures solved in this study are available at http://www.emdataresource.org/ under EMD-50314, EMD-18478 and EMD-50307 (Supplemental Table 2).

The MD data that support the findings of this study, including Supplemental Videos 1 & 2, are available in MD_P116 at https://doi.org/10.5281/zenodo.11941911.

Acknowledgements and Funding

We thank the Frankfurt Center for Electron Microscopy and the Frankfurt Center for Advanced Light Microscopy for measurement time. We thank the Central Electron Microscopy Facility at the MPI of Biophysics in Frankfurt, which enabled us to collect the tomography dataset as well as the cryo-EM dataset of *empty* P116 monomers, particularly S. Welsch and S. Prinz who assisted during the data collection. We thank N. Morgner and J. Schulte for their support during LILBID mass spectroscopy measurements, C. Glaubitz and I. Weber for assistance with liposome preparation, I. Fita, D. Vizarraga and J. Martín for the kind provision of purified P116 (246–818), M. Kunz for support with tomogram reconstruction, and A. N. Birtasu and U. H. Ermel for assistance with sub-tomogram averaging. We thank Jörg Stülke *for providing the M. pneumoniae* replicating plasmid pGP2756[17]. We thank Ignacio Fita/Jesús Martín for gifting us vector pOPINE_P116. We thank M. R. Vabulas for valuable discussions and comments. S.M. A. and R.C. acknowledge the support of Goethe University Frankfurt, the Frankfurt Institute of Advanced Studies, the LOEWE Center for Multiscale Modelling in Life Sciences of the state of Hesse, the CRC 1507: Membrane-associated Protein Assemblies, Machineries, and Supercomplexes (P09), and the International Max Planck Research School on Cellular Biophysics, as well as computational

resources and support from the Center for Scientific Computing of the Goethe University and the Jülich Supercomputing Centre. A. S. F. acknowledges support from the Deutsche Forschungsgemeinschaft (FR 1653/6-3 for L.S., SFB 902 for K.W. and D.B.) and the Research Training Group iMOL (GRK 2566/1 for S.M).

Author contributions

S.M.: Expressed and purified P116 (30–957), optimized and carried out emptying protocol, established and carried out cargo binding and delivery assays, prepared samples for single-particle analysis, established and cultured P116 overexpression strain of *M. pneumoniae*, prepared samples for tomography, recorded and processed single-particle dataset of empty P116 (246–818) monomers. S.M.A: Planned and carried out all MD simulations and MD data analysis. S.M. and L.S.: Recorded and processed tomography dataset of *M. pneumoniae* P116 overexpression strain. J.M.-C.: Performed mass spectrometry analyses of all samples from cargo binding and delivery assays. K.W. and S.M.: Carried out laser scanning microscopy on samples from delivery assays. D.B.: Assisted with expression and purification of P116 (30–957), emptying and refilling protocols, and cargo binding and delivery assays. J.L., R.C. and A.S.F.: Designed and supervised research. S.M. and A. S. F.: Wrote the manuscript, with contributions from all authors.

Competing interests

The authors declare no competing interests.

References

1. AhYoung, A. P. *et al.* Conserved SMP domains of the ERMES complex bind phospholipids and mediate tether assembly. *Proceedings of the National Academy of Sciences* **112**, (2015).
2. Wang, Y. *et al.* Insights into membrane association of the SMP domain of extended synaptotagmin. *Nat Commun* **14**, 1504 (2023).
3. Schauder, C. M. *et al.* Structure of a lipid-bound extended synaptotagmin indicates a role in lipid transfer. *Nature* **510**, 552–555 (2014).
4. Hughes, G. W. *et al.* Evidence for phospholipid export from the bacterial inner membrane by the Mla ABC transport system. *Nat Microbiol* **4**, 1692–1705 (2019).
5. Ekiert, D. C. *et al.* Architectures of Lipid Transport Systems for the Bacterial Outer Membrane. *Cell* **169**, 273-285.e17 (2017).
6. Sprankel, L. *et al.* Essential protein P116 extracts cholesterol and other indispensable lipids for Mycoplasmas. *Nat Struct Mol Biol* **30**, 321–329 (2023).
7. McElhaney, R. N. & Tourtellotte, M. E. Mycoplasma Membrane Lipids: Variations in Fatty Acid Composition. *Science (1979)* **164**, 433–434 (1969).
8. Archer, D. B. The Structure and Functions of the Mycoplasma Membrane. in 1–44 (1981). doi:10.1016/S0074-7696(08)62319-0.
9. Chen, J. *et al.* Structure of an endogenous mycobacterial MCE lipid transporter. *Nature* **620**, 445–452 (2023).
10. Yus, E. *et al.* Impact of Genome Reduction on Bacterial Metabolism and Its Regulation. *Science (1979)* **326**, 1263–1268 (2009).
11. Gianotti, A. R., Klinke, S. & Ermácora, M. R. The structure of unliganded sterol carrier protein 2 from Yarrowia lipolytica unveils a mechanism for binding site occlusion. *J Struct Biol* **213**, 107675 (2021).
12. Burgardt, N. I., Gianotti, A. R., Ferreyra, R. G. & Ermácora, M. R. A structural appraisal of sterol carrier protein 2. *Biochimica et Biophysica Acta (BBA) - Proteins and Proteomics* **1865**, 565–577 (2017).
13. Srinivasan, S., Lorenzo, D. A. & Vanni, S. Unbiased MD simulations characterize lipid binding to lipid transfer proteins. *bioRxiv* 2023.11.24.568550 (2023) doi:10.1101/2023.11.24.568550.
14. Gaspari, E. *et al.* Model-driven design allows growth of Mycoplasma pneumoniae on serum-free media. *NPJ Syst Biol Appl* **6**, 33 (2020).
15. Casares, D., Escribá, P. V. & Rosselló, C. A. Membrane Lipid Composition: Effect on Membrane and Organelle Structure, Function and Compartmentalization and Therapeutic Avenues. *Int J Mol Sci* **20**, 2167 (2019).
16. Wong, L. H., Gatta, A. T. & Levine, T. P. Lipid transfer proteins: the lipid commute via shuttles, bridges and tubes. *Nat Rev Mol Cell Biol* **20**, 85–101 (2019).
17. Blötz, C. *et al.* Development of a replicating plasmid based on the native oriC in Mycoplasma pneumoniae. *Microbiology (N Y)* **164**, 1372–1382 (2018).
18. Hedreyda, C. T., Lee, K. K. & Krause, D. C. Transformation of Mycoplasma pneumoniae with Tn4001 by Electroporation. *Plasmid* **30**, 170–175 (1993).
19. Schindelin, J. *et al.* Fiji: an open-source platform for biological-image analysis. *Nat Methods* **9**, 676–682 (2012).
20. Mastronarde, D. N. Automated electron microscope tomography using robust prediction of specimen movements. *J Struct Biol* **152**, 36–51 (2005).

21. Punjani, A., Rubinstein, J. L., Fleet, D. J. & Brubaker, M. A. cryoSPARC: algorithms for rapid unsupervised cryo-EM structure determination. *Nat Methods* **14**, 290–296 (2017).
22. Punjani, A., Zhang, H. & Fleet, D. J. Non-uniform refinement: adaptive regularization improves single-particle cryo-EM reconstruction. *Nat Methods* **17**, 1214–1221 (2020).
23. Tegunov, D. & Cramer, P. Real-time cryo-electron microscopy data preprocessing with Warp. *Nat Methods* **16**, 1146–1152 (2019).
24. Kremer, J. R., Mastronarde, D. N. & McIntosh, J. R. Computer Visualization of Three-Dimensional Image Data Using IMOD. *J Struct Biol* **116**, 71–76 (1996).
25. Ermel, U. H., Arghittu, S. M. & Frangakis, A. S. ArtiaX: An electron tomography toolbox for the interactive handling of sub-tomograms in UCSF ChimeraX. *Protein Science* **31**, (2022).
26. Scheres, S. H. W. RELION: Implementation of a Bayesian approach to cryo-EM structure determination. *J Struct Biol* **180**, 519–530 (2012).
27. Pettersen, E. F. *et al.* UCSF Chimera—A visualization system for exploratory research and analysis. *J Comput Chem* **25**, 1605–1612 (2004).
28. Van Der Spoel, D. *et al.* GROMACS: Fast, flexible, and free. *J Comput Chem* **26**, 1701–1718 (2005).
29. Bussi, G., Donadio, D. & Parrinello, M. Canonical sampling through velocity rescaling. *J Chem Phys* **126**, (2007).
30. Guvench, O., Hatcher, E., Venable, R. M., Pastor, R. W. & MacKerell, A. D. CHARMM Additive All-Atom Force Field for Glycosidic Linkages between Hexopyranoses. *J Chem Theory Comput* **5**, 2353–2370 (2009).
31. Guvench, O. *et al.* Additive empirical force field for hexopyranose monosaccharides. *J Comput Chem* **29**, 2543–2564 (2008).
32. Best, R. B. *et al.* Optimization of the Additive CHARMM All-Atom Protein Force Field Targeting Improved Sampling of the Backbone ϕ, ψ and Side-Chain χ_1 and χ_2 Dihedral Angles. *J Chem Theory Comput* **8**, 3257–3273 (2012).
33. Parrinello, M. & Rahman, A. Polymorphic transitions in single crystals: A new molecular dynamics method. *J Appl Phys* **52**, 7182–7190 (1981).
34. Periole, X., Cavalli, M., Marrink, S.-J. & Ceruso, M. A. Combining an Elastic Network With a Coarse-Grained Molecular Force Field: Structure, Dynamics, and Intermolecular Recognition. *J Chem Theory Comput* **5**, 2531–2543 (2009).
35. Qi, Y. *et al.* CHARMM-GUI Martini Maker for Coarse-Grained Simulations with the Martini Force Field. *J Chem Theory Comput* **11**, 4486–4494 (2015).
36. Hsu, P. *et al.* CHARMM-GUI Martini Maker for modeling and simulation of complex bacterial membranes with lipopolysaccharides. *J Comput Chem* **38**, 2354–2363 (2017).
37. Mirdita, M. *et al.* ColabFold: making protein folding accessible to all. *Nat Methods* **19**, 679–682 (2022).
38. Berendsen, H. J. C., Postma, J. P. M., van Gunsteren, W. F., DiNola, A. & Haak, J. R. Molecular dynamics with coupling to an external bath. *J Chem Phys* **81**, 3684–3690 (1984).
39. Wassenaar, T. A., Ingólfsson, H. I., Böckmann, R. A., Tieleman, D. P. & Marrink, S. J. Computational Lipidomics with *insane* : A Versatile Tool for Generating Custom Membranes for Molecular Simulations. *J Chem Theory Comput* **11**, 2144–2155 (2015).